ANALYSIS OF COMPOSITE LAMINATES USING GRAPHICAL PROCESSING

BARROS, J.A.O.
Lecteurer
University of Minho
Braga, Portugal

FIGUEIRAS, J.A.
Professor
University of Porto
Porto, Portugal

SUMMARY

The increased usage of advanced fibrous composite materials in structural engineering has made mandatory the development of computacional models for their analysis. The present model for linear and nonlinear analysis is based on the finite element techniques and deals with plates, slabs or plane shells made of fibrous and laminated composite materials. Parabolic finite elements formulated according to the Mindlin theory are employed. The assumption of constant transverse shear strain is corrected by using a shear correction factor derived in cylindrical bending to approximate the real shear strain energy.

The computacional code, developed for small computers, consists in three basic parts: pré-processing with graphical verification; analysis to obtain the global displacements and reactions for each load case, and finally, post-processing with full graphical output of all quantities of interest for each layer or layer interfaces. Some applications are ilustrated.

1. INTRODUCTION

The present model deals with the linear and the geometrically nonlinear analysis of composite laminates built up by isotropic and orthotropic layers. The laminate structures are discretized by linear and quadratic flat finite elements with five degrees of freedom per node. A Total Lagrangian approach accounting for large displacements in the Von Karman [1] sense is adopted. The solution of the nonlinear equations is performed by using the Newton-Raphson method.

2. NUMERICAL MODEL

2.1 Displacements, strains and stress

The assumed displacement field [2,3] of a $n - ply$ composite laminate has the following form,

$$u(x,y,z) = \overline{u}(x,y) + z\,\theta_y\,(x,y) \tag{1}$$

$$v(x,y,z) = \overline{v}(x,y) - z\,\theta_x\,(x,y) \tag{2}$$

$$w(x,y,z) = \overline{w}(x,y) \tag{3}$$

in which $\overline{u}, \overline{v}$ and $\overline{w}$ are the midplane displacements and θ_x, θ_y are de rotations of a normal to the midplane with relation to the x and y axis, respectively.

The strain vector [4] accounting for large displacements, small rotations and infinitesimal strains is written by the relation,

$$\underline{\varepsilon} = \underline{\overline{\varepsilon}}_0 + \underline{\overline{\varepsilon}}_L \tag{4}$$

wherein

$$\underline{\overline{\varepsilon}}_0 = \left\{ \begin{array}{c} \underline{\overline{\varepsilon}}^m \\ \cdot \\ \underline{\overline{\varepsilon}}^c \end{array} \right\} + z \left\{ \begin{array}{c} \underline{\overline{\varepsilon}}^f \\ \cdot \\ \underline{0} \end{array} \right\} \tag{5}$$

with

$$\underline{\overline{\varepsilon}}^m = \left\{ \begin{array}{c} \frac{\partial \overline{u}}{\partial x} \\ \\ \frac{\partial \overline{v}}{\partial y} \\ \\ \frac{\partial \overline{u}}{\partial y} + \frac{\partial \overline{v}}{\partial x} \end{array} \right\} ; \underline{\overline{\varepsilon}}^c = \left\{ \begin{array}{c} \theta_y + \frac{\partial \overline{w}}{\partial x} \\ \\ -\theta_x + \frac{\partial \overline{w}}{\partial y} \end{array} \right\} ; \underline{\overline{\varepsilon}}^f = \left\{ \begin{array}{c} \frac{\partial \theta_y}{\partial x} \\ \\ -\frac{\partial \theta_x}{\partial y} \\ \\ \frac{\partial \theta_y}{\partial y} - \frac{\partial \theta_x}{\partial x} \end{array} \right\} \tag{6}$$

corresponding to the membrane, shear and bending strains, respectively, and,

$$\underline{\overline{\varepsilon}}_L = \left\{ \begin{array}{c} \frac{1}{2}\left(\frac{\partial \overline{w}}{\partial x}\right)^2 \\ \\ \frac{1}{2}\left(\frac{\partial \overline{w}}{\partial y}\right)^2 \\ \\ \frac{\partial \overline{w}}{\partial x} \cdot \frac{\partial \overline{w}}{\partial y} \end{array} \right\} \tag{7}$$

represents the membrane nonlinear strains.

The Piola-Kirchhoff stress vector [5], corresponding to the Green-Lagrange strain vector is given by,

$$\underline{\overline{\sigma}}^m = \{N_x, N_y, N_{xy}\}^T = \left[\int_{-h/2}^{h/2} (\sigma_x, \sigma_y, \tau_{xy})\, dz\right]^T \tag{8}$$

$$\underline{\overline{\sigma}}^f = \{M_{xx}, M_{yx}, M_{xy}\}^T = \left[\int_{-h/2}^{h/2} (\sigma_x, \sigma_y, \tau_{xy})\, .z.dz\right]^T \tag{9}$$

$$\underline{\overline{\sigma}}^c = \{Q_{xz}, Q_{yz}\}^T = \left[\int_{-h/2}^{h/2} (\tau_{xz}, \tau_{yz})\, dz\right]^T \tag{10}$$

for the membrane, bending and shear stress resultants.

2.2 The Generalized Hooke's Law

The stress-strain relations for the k^{th} layer in the material coordinate axes (x, y, z) are written as

$$\underline{\sigma}_k = \begin{Bmatrix} \overline{\sigma} \\ \cdots \\ \overline{\tau} \end{Bmatrix}_k = \begin{bmatrix} [D_1] & \vdots & [0] \\ \cdots & \cdots & \cdots \\ [0] & \vdots & [D_2] \end{bmatrix}_k \left[\begin{Bmatrix} \overline{\varepsilon}^m \\ \cdots \\ \overline{\varepsilon}^c \end{Bmatrix} + z_k \begin{Bmatrix} \overline{\varepsilon}^f \\ \cdots \\ \underline{0} \end{Bmatrix} + \begin{Bmatrix} \overline{\varepsilon}_L \\ \cdots \\ \underline{0} \end{Bmatrix} \right] \tag{11}$$

wherein

$$[D_1]_k = [T_1]_k^T \, [C_1]_k \, [T_1]_k \tag{12}$$

$$[D_2]_k = [T_2]_k^T \, [C_2]_k \, [T_2]_k \tag{13}$$

and

$$[T_1]_k = \begin{bmatrix} \cos^2\theta & \sin^2\theta & 2\sin\theta\cos\theta \\ \sin^2\theta & \cos^2\theta & -2\sin\theta\cos\theta \\ -\sin\theta\cos\theta & \sin\theta\cos\theta & \cos^2\theta - \sin^2\theta \end{bmatrix} \tag{14}$$

$$[T_2]_k = \begin{bmatrix} \cos\theta & \sin\theta \\ -\sin\theta & \cos\theta \end{bmatrix} \tag{15}$$

represent the transformation matrices between the local and the global coordinate systems, and θ corresponds to the angle between the global x axis and the fibers orientations (anticlockwise).

The elasticity matrices for the k^{th} layer corresponding to the normal and shear strains, respectively, are written as

$$[C_1]_k = \begin{bmatrix} C_{11} & C_{12} & 0 \\ C_{21} & C_{22} & 0 \\ 0 & 0 & C_{33} \end{bmatrix}_k \; ; \; [C_2]_k = \begin{bmatrix} C_{44} & 0 \\ 0 & C_{55} \end{bmatrix}_k \tag{16}$$

in which

$$\begin{aligned} C_{11} &= E_1/(1 - \nu_{12} \cdot \nu_{21}); & C_{33} &= G_{12}; \\ C_{12} &= C_{21} = \nu_{12} \, E_2/(1 - \nu_{12} \cdot \nu_{21}); & C_{44} &= G_{13} \cdot k_{13}; \\ C_{22} &= E_2/(1 - \nu_{12} \cdot \nu_{21}); & C_{55} &= G_{23} \cdot k_{23}, \end{aligned} \tag{17}$$

The shear correction factors k_{13} and k_{23} [3,6–8] are introduced in (17) to correct the constant shear strain hyphotesis of the Mindlin theory [2] in order to better approximate the real shear strain energy.

2.3 Strain matrix

According to (4), the differential operators relating strains to displacements are written as

$$[B] = [B_0] + [B_L] \tag{18}$$

in wich $[B_0]$ is the strain matrix corresponding to the linear strains $\underline{\varepsilon}_0$,

$$[B_0] = \begin{bmatrix} [B^m] & [0] \\ [0] & \left[B^f\right] \\ [0] & [B^c] \end{bmatrix} \tag{19}$$

and

$$[B^m] = \begin{bmatrix} \frac{\partial N}{\partial x} & 0 \\ 0 & \frac{\partial N}{\partial y} \\ \frac{\partial N}{\partial y} & \frac{\partial N}{\partial x} \end{bmatrix} \; ; \; \left[B^f\right] = \begin{bmatrix} 0 & 0 & \frac{\partial N}{\partial x} \\ 0 & -\frac{\partial N}{\partial y} & 0 \\ 0 & -\frac{\partial N}{\partial x} & \frac{\partial N}{\partial y} \end{bmatrix} \; ; \; [B^c] = \begin{bmatrix} \frac{\partial N}{\partial x} & 0 & N \\ \frac{\partial N}{\partial y} & -N & 0 \end{bmatrix} \tag{20}$$

are the membrane, bending and shear strain-displacement matrices, respectively.

The nonlinear strain matrix is expressed by,

$$[B_L] = \begin{bmatrix} [0] & \left[B_L^f\right] \\ [0] & [0] \\ [0] & [0] \end{bmatrix} \tag{21}$$

wherein

$$\left[B_L^f\right] = [A]\,[G] \tag{22}$$

and

$$[A] = \begin{bmatrix} \frac{\partial w}{\partial x} & 0 \\ 0 & \frac{\partial w}{\partial y} \\ \frac{\partial w}{\partial y} & \frac{\partial w}{\partial x} \end{bmatrix} \; ; \; [G] = \begin{bmatrix} \frac{\partial N}{\partial x} & 0 & 0 \\ \frac{\partial N}{\partial y} & 0 & 0 \end{bmatrix} \tag{23}$$

where N are the shape functions [10].

2.4 Stiffness matrix

The nonlinear equilibrium equations can be expressed by,

$$d\underline{\psi} = [k_T]\, d\underline{U} \tag{24}$$

in which $d\underline{\psi}$ represents the residual generalized forces, and $[k_T]$ the tangencial stiffness matrix,

$$[k_T] = [k_0 + k_L + k_\sigma] \tag{25}$$

and $d\underline{U}$ the nodal displacement increment.

The submatrices $[k_0]$, $[k_L]$ and $[k_\sigma]$ correspond to the small displacement (linear analysis), large displacement and geometric matrices, respectively.

Incorporating (4) and (11) in the virtual work principle, $dW_i = \int_v d\underline{\varepsilon}^T \underline{\sigma} dv$, developing the implicit matrix products and integrating through the laminate thickness, the components of the stiffness matrix $[k_0 + k_L]$ are obtained [3].

The geometric stiffness matrix $[k_\sigma]$ is given by,

$$[k_\sigma] = \int_A [G]^T [M] [G] \, dA \tag{26}$$

in which

$$[M] = \begin{bmatrix} N_x & N_{xy} \\ N_{xy} & N_y \end{bmatrix} \tag{27}$$

The vector of nodal forces equivalent to the internal stress field is obtained by

$$\overline{F} = \int_A \begin{Bmatrix} [B^m]^T \overline{\sigma}^m \\ \left[B_L^f\right]^T \overline{\sigma}^m + \left[B^f\right]^T \overline{\sigma}^f + [B^c]^T \overline{\sigma}^c \end{Bmatrix} dA \tag{28}$$

2.5 Nonlinear solution algorithm

The solution of the equilibrium equations is performed by an incremental and iterative procedure. In the present model the Newton-Raphson method [11] is adopted with different schemes. Two convergence criteria have been employed: i) displacement convergence criteria; ii) force convergence criteria.

3. COMPUTER CODE

The computer codes for the linear and the geometric nonlinear analysis have similar structure, consisting in three modules:

i) The pre-processing module generates the finite element mesh, and creates the corresponding data file. Verification of data is made possible by several graphical facilities.

ii) The solution module calculates the displacements and reactions for each load case (linear analysis) or for each load increment (geometric nonlinear analysis). The results are kept in unfformatted files in order to minimize memory space allocation.

iii) The post-processing module have different options which allow graphic or numerical output for each load case (or load increment). The results may be obtained in the middle surface or interfaces of each laminate layer. The optional output facilities provide computer memory and time savings.

4. NUMERICAL EXAMPLES AND DISCUSSION

The appraisal of the present finite element formulation has already been estabilished by comparing its results with those available in several references [4,5,8,12–17]. In the following numerical examples the solution performance and the graphical possibilities are illustrated.

4.1 Composite table

The first example is a part of a research project, looking for the appropriated design of seats for trains. The table, component of seats (Fig. 1) is built by seven plies, stacked as shown in Fig. 2.. The material properties of plies are presented in table 1. The composite table was discretized by 24 eight-node Serendipity finite elements mesh (Fig. 3) and linear elastic analysis is adopted.

By simmetry considerations, only a half of the plate is discretized, Fig. 3. The boundary conditions associated to a cantilever plate and the vertical force ($850N$) in the nineth node are also shown.

In figures 4 to 6 are presented in graphic shape some of the results which illustrate that the structure will perform correctly under the assumptions of ultimate stress level and service working conditions.

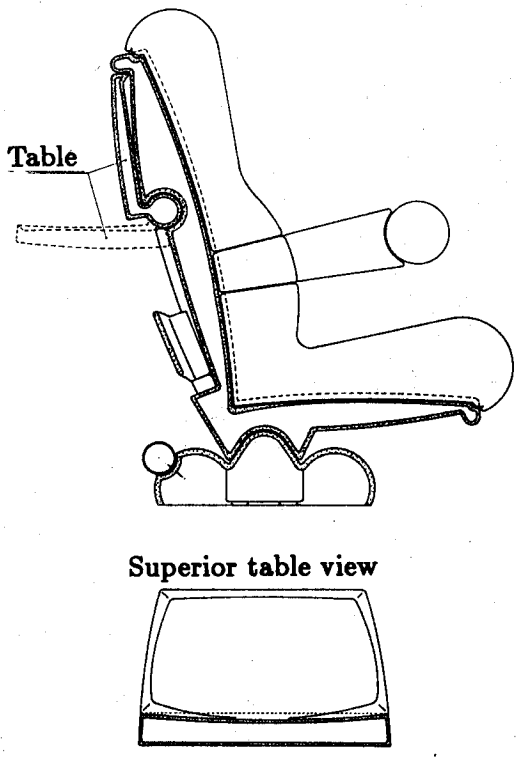

Fig. 1 – Composite table

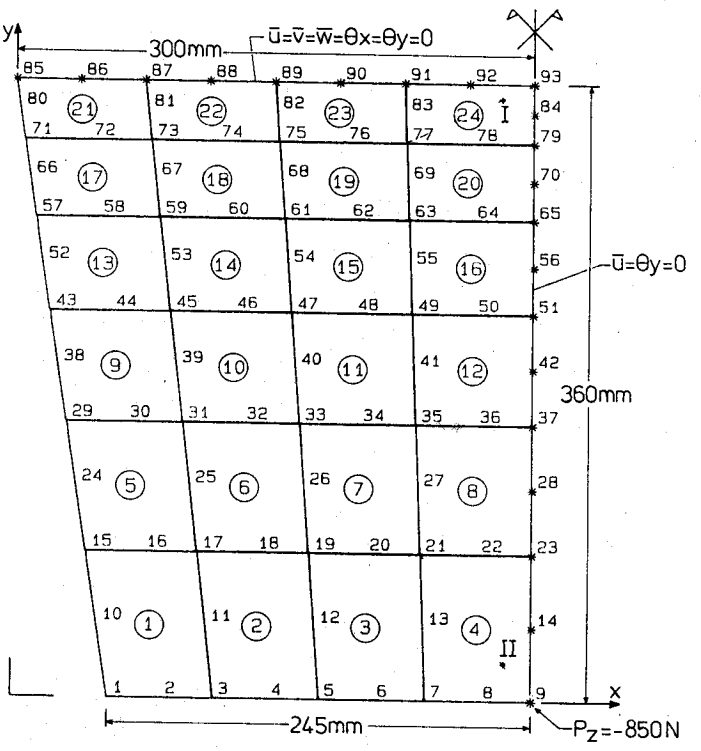

Fig. 3 – Finite element mesh

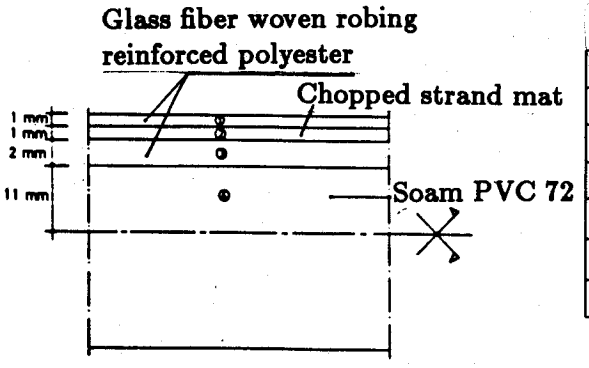

Fig. 2 – Transversal section

	Glass fiber woven robing reinforced poliester	Chopped strand mat		Soam Pvc 72
E_1 (MPa)	24740	11000	E (MPa)	72.6
E_2 (MPa)	24740	11000	G (MPa)	19.3
G (MPa)	4500	4300	σ (MPa)	4.08
σ (MPa)	338	159	τ (MPa)	2.16
τ (MPa)	100	50	ρ (N/mm^3)	0.13×10^{-5}
ρ (N/mm^3)	0.15×10^{-4}	0.15×10^{-4}	ν	0.3
ν	0.18	0.31		

Table 1 – Material properties of plies

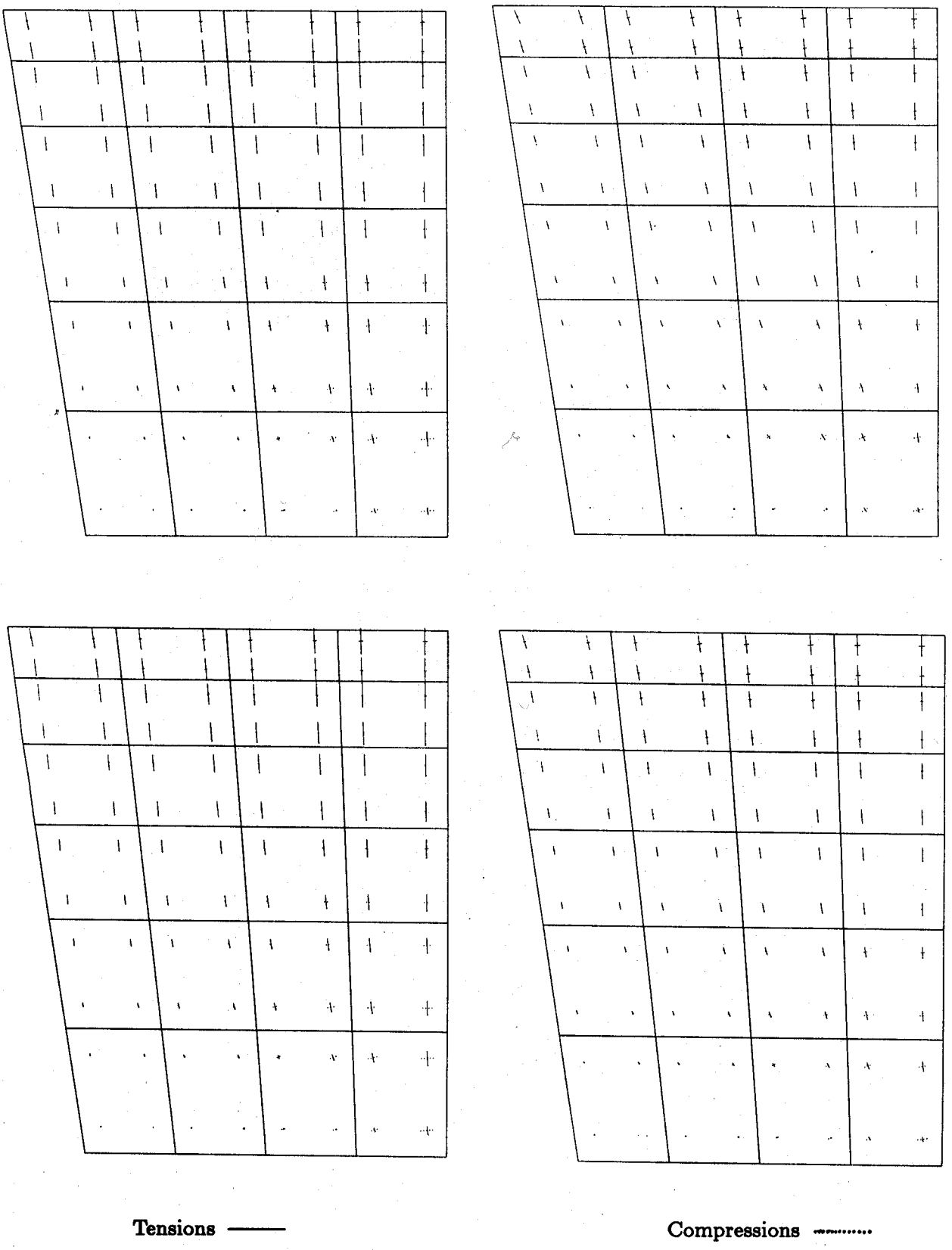

Fig. 4 – Principal stresses: a) Top surface of 1*st* ply ($\sigma_{max} = 15.3\,MPa$); b) Top surf. of 2*nd* ply ($\sigma_{max} = 6.8\,MPa$); c) Top surf. of 3*rd* ply ($\sigma_{max} = 13.3\,MPa$); d) Top surf. of 4*th* ply ($\sigma_{max} = 0,035\,MPa$).

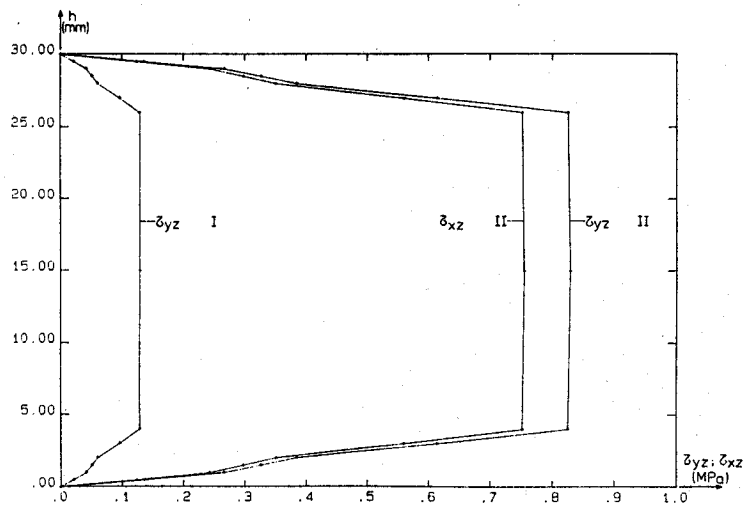

Fig. 5 – Shear stresses in I and II Gauss Points

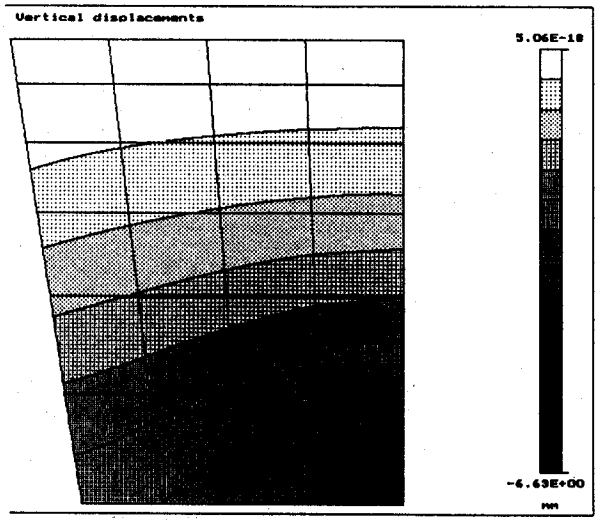

Fig. 6 – Vertical displacement field

4.2 Orthotropic square plate

4.2.1 Clamped plate

The geometrically nonlinear analysis of an orthotropic plate (Fig. 7) under a uniform transverse pressure is carried out and compared with results given by other authors. The material properties and parameters used are as follows:

– $E_2/E_1 = 3.0$; $\nu_{12} = 0.25$; $\dfrac{G_{12}}{E_1} = \dfrac{G_{13}}{E_1} = \dfrac{G_{23}}{E_1} = 0.50$.

– Nine - node Lagrange elements.
– Reduced integration.
– Specified tolerance of 0.1% according to the force convergence criteria.
– Newton - Raphson method with stiffness matrix updated in each iteration.

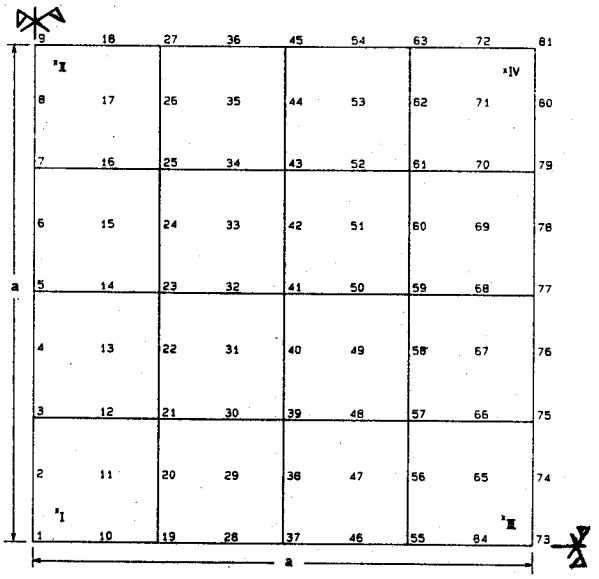

Fig. 7 – Orthotropic square plate (mesh)

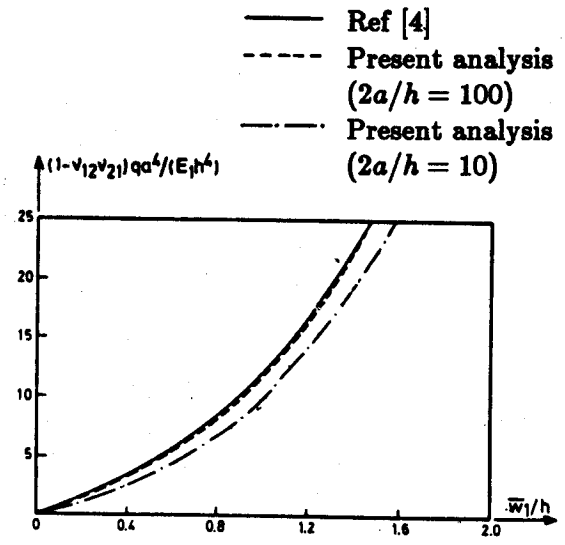

Fig. 8 – Normalized central (1*st* node) displacement variation with load parameter.

4.2.2 Simply supported square plate

The orthotropic plate (Fig. 7) under a uniform transverse pressure, with the same parameters and material properties of 4.2.1 is now analysed by considering simply supported boundary conditions. The results presented were obtained for thickness/span relation, $2a/h = 10$.

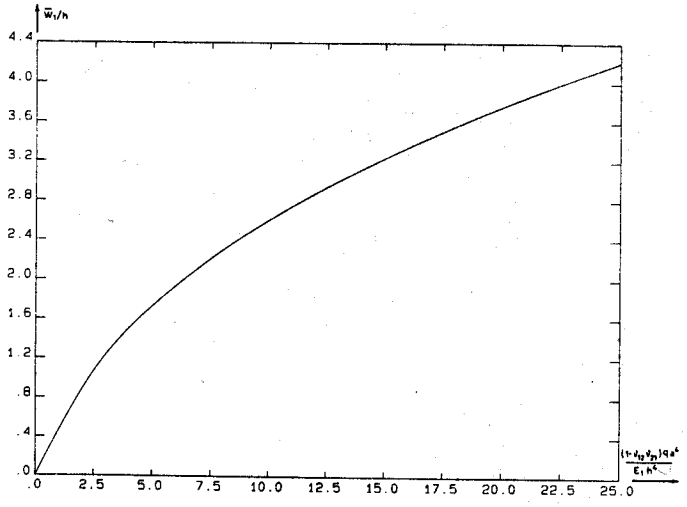

Fig. 9 – Normalized central (1*st* node) displacement variation with load parameter.

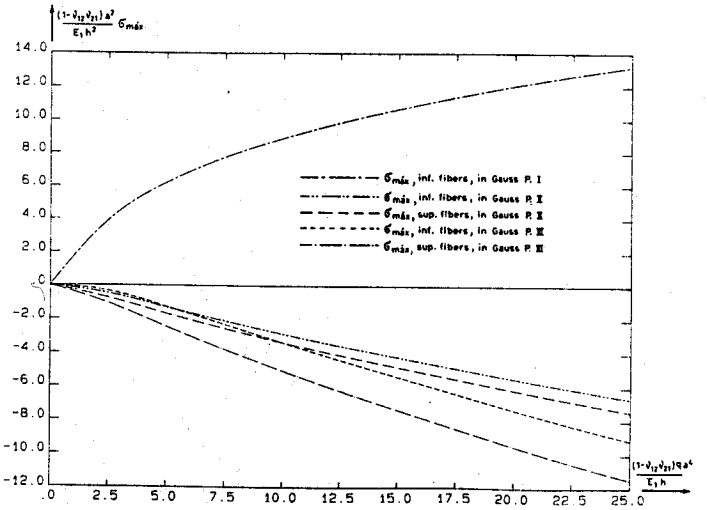

Fig. 10 – Normalized maximum stresses variation with load parameter.

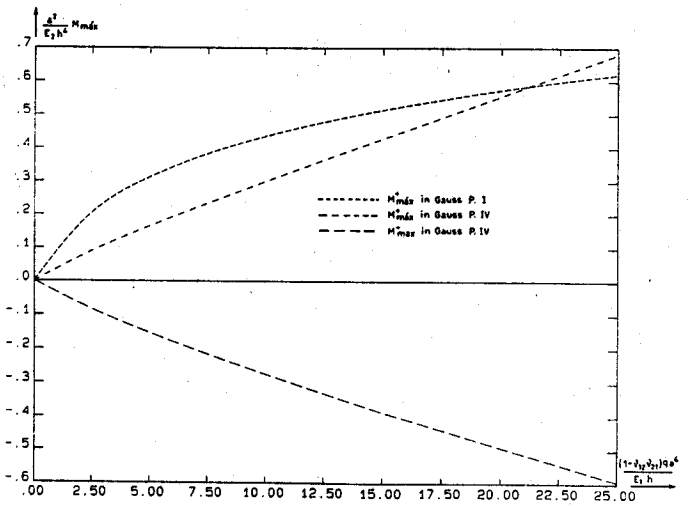

Fig. 11 – Normalized moments variation with load parameter.

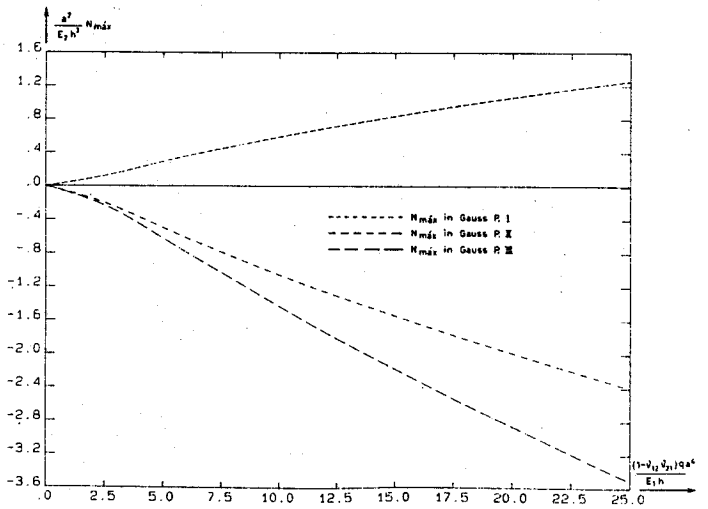

Fig. 12 – Normalized membrane forces variation with load parameter.

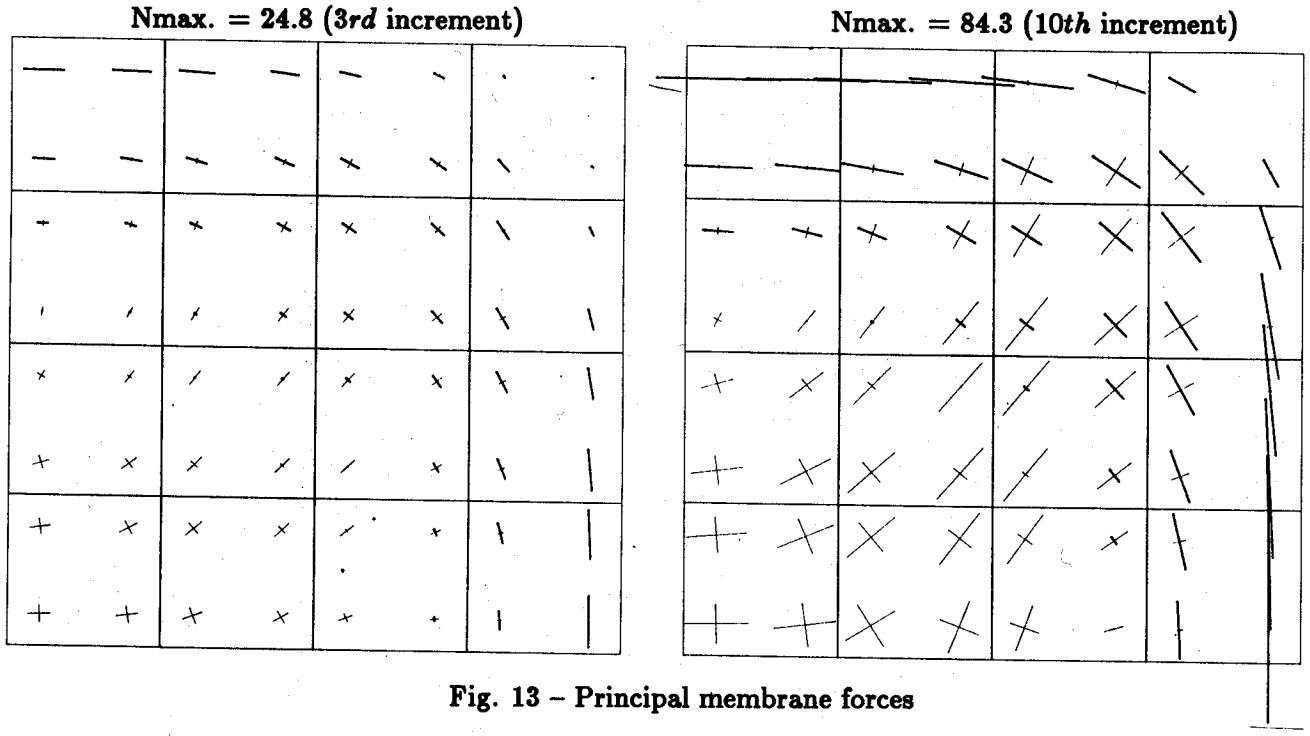

Fig. 13 – Principal membrane forces

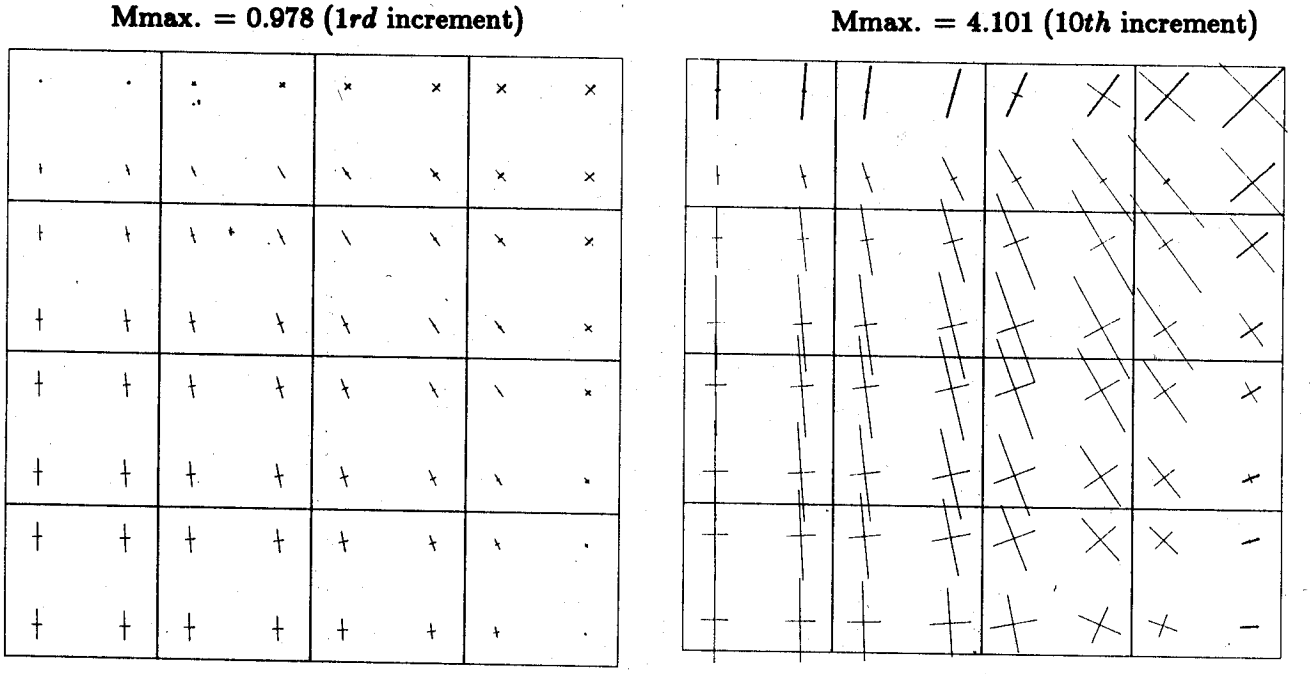

Fig. 14 – Principal moments

Positive moments ——— Negative moments ———

The increasing of stiffness ($[k_L] + [k_\sigma]$) developed with loading leads to the nonlinear variation of vertical displacements (Fig. 9). The stresses (Fig. 10) and the bending moments (Fig. 11), at centre, show as well, a significative nonlinear behaviour. At the zones near the support edges the stress and stress resultants (Figs. 10 to 12) behave approximately in a linear manner. The principal in-plane forces represented in Fig. 13, develop a compressive ring near the support edges which balances the membrane tensile forces in the central zone of the plate.

This ring mechanism leads to the development of negative bending moments mainly, in the fiber direction (Fig. 14). The graphical output illustrated in figure 15 can clarify the previous interpretation.

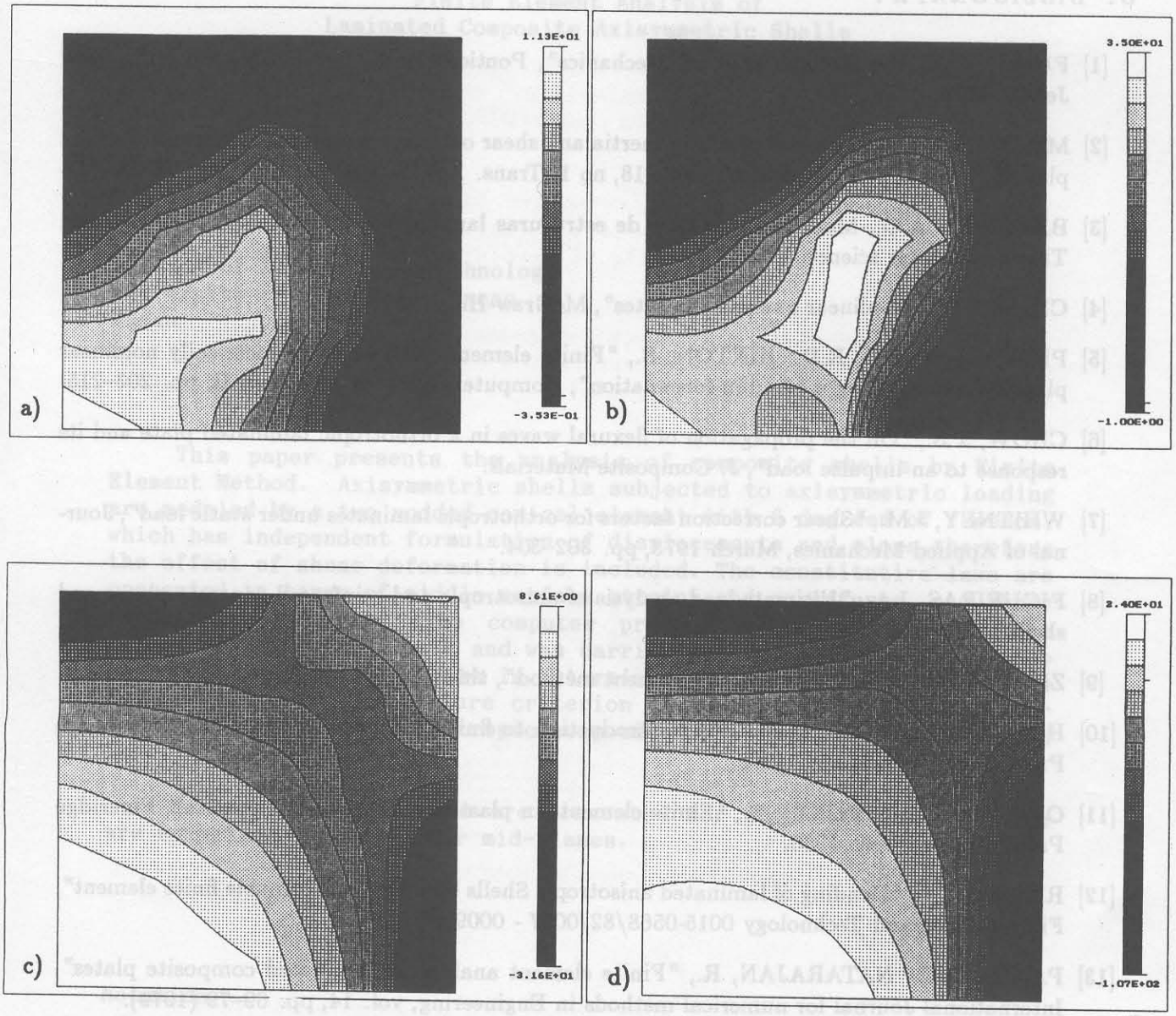

Fig. 15 – Maximum principal membrane forces (positive) at 3*rd* (a) and 10*th* (b) increment
Minimum principal membrane forces (negative) at 3*rd* (c) and 10*th* (d) increment

5. CONCLUDING REMARKS

A model for the linear and geometrically nonlinear analysis of fiber reinforced and composite laminated plates was described. The computational code is implemented with pré- and post-processing graphic facilities which prove to be essencial for the analysis and design of composite structures.

An adequate formulation to take into account the shear deformation and an efficient approach for large displacement analysis which have significant influence on the structural behaviour of composite plates are considered in the present model.

6. BIBLIOGRAPHY

[1] FUNG, Y.G.,"Foundations of Solid Mechanics", Pontice - Hall, Inc. Englwood cliffs, New Jersey, 1965.

[2] MINDLIN, R.D., "Influence of rotary inertia and shear on flexural motions of isotropic, elastic plates", Journal of applied Mech., vol. 18, no 1, Trans. ASME, vol. 73, 1951, pp. 31–38.

[3] BARROS, J.A.O., Modelos de análise de estruturas laminares e de compósitos laminados", Thesis of Master science, 1989.

[4] CHIA, C.Y., "Nonlinear analysis of plates", McGraw-Hill, 1980.

[5] PICA, A.; WOOD, R.D.; HINTON, E., "Finite element analysis of geometrically nonlinear plate behaviour using a Mindlin formulation", Computers & Structures, vol. II, pp. 203–215.

[6] CHOW, T.S., "On the propagation of flexural waves in a orthotropic laminated plate and its response to an impulse load", J. Composite Materials.

[7] WHITNEY, J.M., "Shear correction factors for orthotropic laminates under static load", Journal of Applied Mechanics, March 1973, pp. 302–304.

[8] FIGUEIRAS, J.A., "Ultimate load analysis of anisotropic and reinforced concrete plates and shells", Ph. D. thesis, Swansea, 1983.

[9] ZIENKIEWICZ, O.C., "The finite element method", third edition, MacGraw-Hill, 1977.

[10] HINTON, E.; OWEN, D.R.J., "An introduction to finite element computations", Pineridge Press Limited, Swansea, U.K..

[11] OWEN, D.R.J.; HINTON, E., "Finite elements in plasticity - theory and pratice", Pineridge Press Limited, U.K. 1980.

[12] REDDY, J.N., "Bending of laminated anisotropic Shells by a shear deformable finite element", Fibre Science and Technology 0015-0568/82/0017 - 0009.

[13] PANDA, S.C.; NATARAJAN, R., "Finite element analysis of laminated composite plates", International Journal for numerical methods in Engineering, vol. 14, pp. 69–79 (1979).

[14] ASHTON, J.E., "Clamped Skew plates of orthotropic material under transversal load", Developments in mechanics, vol. 5, procedings of the 11th Midwestern Mechanics Conference.

[15] PAGANO, N.J., "Exact solutions for rectangular bidimensional composite and sandwish plates", J. Composites Materials, vol. 4 (January 1970), pp. 20–34.

[16] PAGANO, N.J., "Exact solutions for composite laminates in cylindrical bending", J. Composite Materials, vol. 3 (July 1969), pp. 398–411.

[17] REDDY, J.N., "A refined nonlinear theory of plates with transverse shear deformation", Int. J. Solids Structures, vol. 20, no 9/10, pp. 881–896, 1984.